# Operando NMR Visualization of Ion Dynamics in PEDOT:PSS

**Yanting Jin**
University of Cambridge
**Pieter Magusin**
University of Cambridge
**Simone Sturniolo**
Science and Technology Facilities Council
**Evan Wenbo Zhao**
University of Cambridge
**Dongxun Lyu**
University of Cambridge
**Shunsuke Yamamoto**
Tohoku University
**George Malliaras**
University of Cambridge https://orcid.org/0000-0002-4582-8501
**Clare Grey** ( cpg27@cam.ac.uk )
University of Cambridge https://orcid.org/0000-0002-6867-6715

**Article**

**Keywords:** ion dynamics, NMR spectroscopy, physical chemistry, polymer chemistry

**Posted Date:** May 14th, 2021

**DOI:** https://doi.org/10.21203/rs.3.rs-493302/v1

# Operando NMR Visualization of Ion Dynamics in PEDOT:PSS

Yanting Jin[1], Pieter C. M. M. Magusin[1],
Simone Sturniolo[2], Evan Wenbo Zhao[1], Dongxun Lyu[1], Shunsuke Yamamoto[3,4],
George G. Malliaras[3], Clare P. Grey[1]

[1]Department of Chemistry, University of Cambridge, Cambridge CB2 1EW, UK
[2]Science and Technology Facilities Council, Harwell Science and Innovation Campus, Didcot, OX11 0QX, UK
[3]Electrical Engineering Division, Department of Engineering, University of Cambridge, Cambridge CB3 0FA, UK
[4]Institute of Multidisciplinary Research for Advanced Materials (IMRAM), Tohoku University, 2-1-1 Katahira, Sendai 9808577, Japan

**Abstract**

While organic mixed ionic/electronic conductors are widely studied for various applications in bioelectronics, energy generation/storage, and neuromorphic computing, a fundamental understanding of the interactions between the ionic and electronic carriers remains unclear, particularly in the wet state and on electrochemical cycling. Here, we show that *operando* NMR spectroscopy can selectively probe and quantify ion and water movement during the doping/dedoping of poly(3,4-ethylene dioxythiophene) poly(styrene sulfonate) (PEDOT:PSS) films, the most widely used organic mixed conductor. $Na^+$ ions near or within the PEDOT-rich domains experience an anisotropic environment resulting from the underlying partial PSS chain orientation in the polymer films, giving rise to a distinct quadrupolar splitting in the $^{23}Na$ NMR spectrum. Operando $^{23}Na$ NMR studies reveal a linear correlation between the quadrupolar splitting and the charge stored in the film, which is interpreted in terms of the roles that the $Na^+$ ions at the PEDOT/PSS interfaces play in charge balance and electric double layer formation. The observed correlation is quantitatively explained by a competitive binding model, in which holes on the PEDOT backbone are bound to PSS, the hole concentration changes during doping/dedoping inducing variations in the $Na^+$ binding percentage at the PEDOT/PSS interfaces. The $Na^+$-to-electron coupling efficiency, measured via $^{23}Na$ NMR intensity changes, varies noticeably depending on the cycling history of the film. Operando $^1H$ NMR spectroscopy confirms that water molecules accompany the ions that are injected into/extracted from the films. These findings shed light on the working principles of organic mixed conductors and demonstrate the utility of operando NMR spectroscopy in revealing structure-property relationships in electroactive polymers.

## Introduction

The design and optimisation of organic materials with mixed ionic and electronic conductivity is key to enabling the next generation of bioelectronic devices, where these materials mediate the coupling between solid-state electronics and biological media for advanced healthcare monitoring and disease treatment.[1,2] Organic mixed conductors are also used as active electrodes[3], electrode coating layers[4] as well as polymer binders in supercapacitors and lithium ion batteries,[5] to improve the electrode conductivity and minimize side-reactions. Moreover, these materials draw significant interest in the facile-to-fabricate, and hence low-cost electronic circuits, that are needed to realise the Internet of Things.[6,7] Finally, the recent development of neuromorphic devices based on organic mixed conductors holds great promise in new computing architectures with improved energy efficiency and biocompatibility.[8,9]

Poly(3,4-ethylene dioxythiophene) doped with poly(styrene sulfonate) (PEDOT:PSS) is the most ubiquitous of all organic mixed ionic/electronic conductors. It is a degenerately doped *p*-type semiconductor, in which holes on the PEDOT chains are compensated by sulfonate anions on the PSS chains. Typical films contain excess PSS and the majority of the sulfonate groups are compensated by cations such as $Na^+$ or $H^+$. PEDOT:PSS films can be dedoped electrochemically under the influence of a voltage that extracts holes through a metal electrode and injects cations from an electrolyte to compensate the "free" $SO_3^-$ groups. Application of the opposite voltage leads to further doping of the film, via the extraction of cations and injection of holes to compensate the free $SO_3^-$ groups. This exchange between holes and cations as the compensating species for $SO_3^-$ takes place at PEDOT/PSS interfaces throughout the bulk of the film and manifests itself as a volumetric capacitance.[10] The morphology of PEDOT:PSS films is controlled via its deposition from dispersions containing colloidal particles with PEDOT-rich cores and PSS-rich coronas (Figure 1a-c).[11] These particles flatten out when spin-casted onto a flat substrate, forming oblate-spheroid, or "pancake-shaped" PEDOT-rich domains, embedded in a PSS-rich matrix. Cross-sectional atomic force microscopy images reveals that the PEDOT-rich domains are typically 20–30 nm in diameter and 4–6 nm in height,[12] containing comparable amounts of PEDOT and PSS as revealed by X-ray scattering[13], with the excess PSS giving rise to the PSS-rich matrix. Films, therefore, show anisotropic electronic (through interconnected PEDOT-rich domains) and ionic (predominantly within the PSS-rich matrix) conduction pathways.[13–16]

PEDOT:PSS has been traditionally used in optoelectronics as a hole-conducting layer.[17] While electronic charge carrier transport in this material in the dry-state is reasonably well understood, the ion-polymer interactions and ion-electron coupling within the conjugated

polymer in the wet-state and during device operation have not been studied with equal depth.[10,18,19] This is mainly due to challenges in monitoring molecular and electronic structure in a heterogeneous polymer matrix and in differentiating between electronic and ionic charge carriers using traditional electrical techniques alone. It is of interest to differentiate and quantify each process, as the competing absorption of $Na^+$ and $H^+$ in PEDOT:PSS induces a local pH change, which may affect the stability of the polymer or the viability of cells in biological interfaces.[20,21] Various characterization techniques have been reported to analyse the ion injection/extraction process during dedoping/doping. Electrochemical quartz crystal microbalance with dissipation monitoring (EQCM-D) has been used to measure the change in mass per injected cation,[22] however, an accurate estimate of the ionic-to-electronic coupling efficiency from this measurement requires independent knowledge concerning both the nature of the ions and the number of water molecules in their hydration shells involved in the electrochemical processes. Ion transport in conjugated polymers has been probed by the moving front method using time-lapse optical micrographs,[19] which revealed fast cation drift mobility in PEDOT:PSS films. This method, however, cannot differentiate between species (e.g., $Na^+$ from $H^+$), nor can it quantify the relative strength of coupling between different charge species. New, quantitative techniques are needed to understand ion injection and transport, their coupling to electronic conductivity, and polymer film structure.

Nuclear magnetic resonance (NMR) spectroscopy is a non-invasive and nuclei-specific technique that can provide both quantitative atomic and dynamic information.[23–26] Operando NMR spectroscopy in particular has been applied to study various battery materials to provide structural and dynamic information concerning transient species.[27] Here, operando $^{23}Na$ and $^{1}H$ NMR spectroscopies are used to understand the ion and water movement within the PEDOT:PSS film. The film was cross-linked with 1 wt % 3-glycidoxypropyltrimethoxysilane (GOPS) to prevent the film dissolving in the aqueous electrolyte. We exploit the quadrupolar nature of the $^{23}Na$ nucleus, the quadrupolar interaction between the nucleus and the electric field gradient (EFG) tensor at the nucleus being a sensitive measure of the anisotropy of the $Na^+$ environments[28,29] in heterogenous polymer films. Operando $^{23}Na$ NMR studies show that the quadrupolar splitting, extracted from the quadrupolar lineshape, is negatively correlated with the number of ions stored in the film, the correlation being explained by the injection/extraction of $Na^+$ near PEDOT/PSS interfaces. The $Na^+$-to-electron coupling efficiency is quantified via integration of the operando NMR signals. The methods demonstrated here open further possibilities to understand the mechanisms, capacity retention and degradation of mixed ionic and electronic conducting polymers.

## Results

### $^{23}$Na NMR reveals two Na$^+$ environments and partial orientation in the polymer

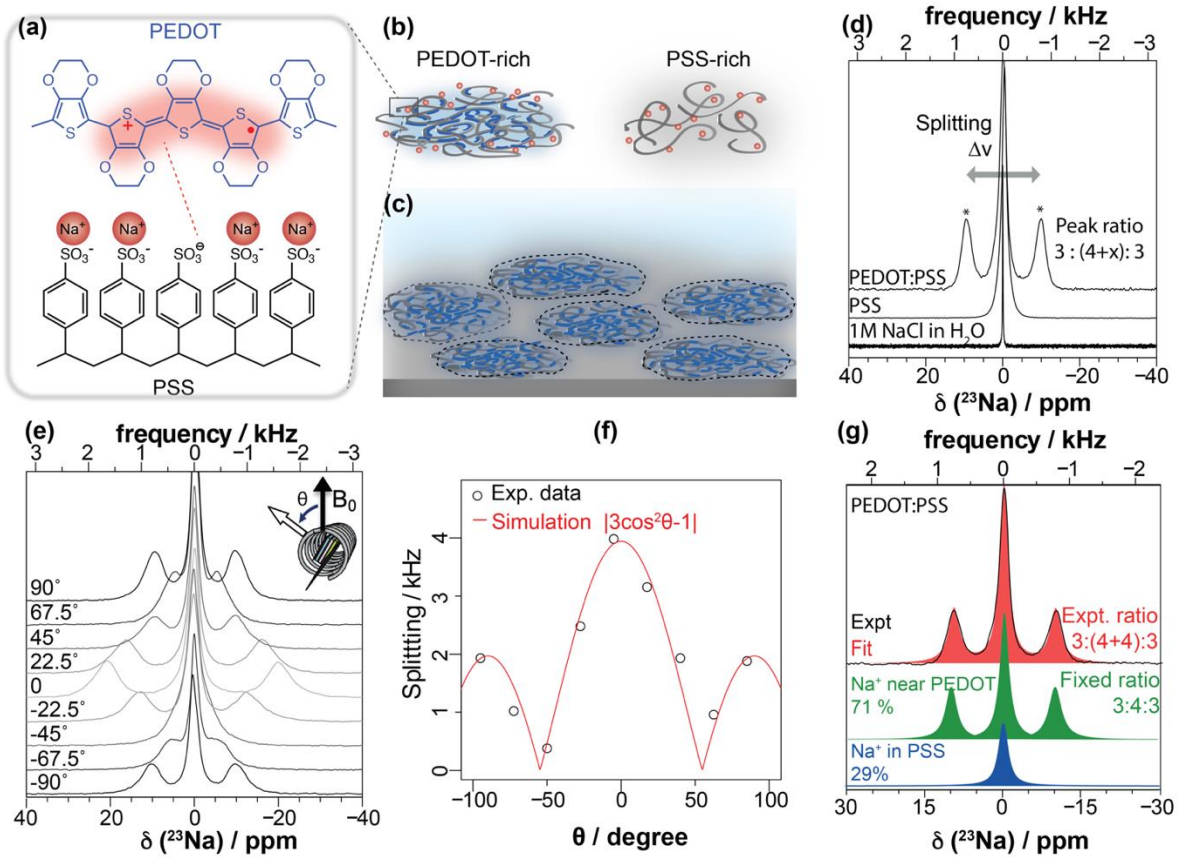


***Figure 1. Na$^+$ binding sites in PEDOT:PSS and their measurement via $^{23}$Na NMR spectroscopy.*** *a) Chemical structure of PEDOT:PSS. The negatively charged $SO_3^-$ groups on PSS are charge compensated by (red) Na$^+$ or H$^+$ ions, or by holes on PEDOT chains that are in close contact to PSS, as illustrated by the red dashed line. A hole polaron on PEDOT (shaded in red) is formed by three EDOT units. (b-c) Schematic of a wet PEDOT:PSS film based on the model in Ref.*[13]*. PEDOT and PSS chains form "pancake"-shaped PEDOT-rich domains (circled by dashed lines), embedded in a PSS-rich matrix (grey). (d) $^{23}$Na NMR spectra of PEDOT:PSS and PSS polymer films soaked in a 1M NaCl solution. Both films are oriented vertically in the magnetic field $B_0$ (i.e.,* with a value for $\theta$, the angle between the film normal and $B_0$, of 90°. *The PEDOT:PSS spectrum shows satellite peaks (*) separated by a frequency difference $\Delta\nu$. (e) The effect of film orientation on the $^{23}$Na NMR spectra. (f) Satellite peak frequency separation $\Delta\nu$ versus film orientation $\theta$. The data points are extracted from (e) and the continuous line represents a fit to the function $\Delta\nu = \frac{1}{2}\langle\bar{\chi}\rangle\,|3\cos^2\theta - 1|$ with a residual quadrupole coupling constant $\langle\bar{\chi}\rangle$ of ca. 4 kHz. (g) Deconvolution of the $^{23}$Na NMR spectrum of a PEDOT:PSS film into two components: Na$^+$ near PEDOT-rich region with fixed peak ratio of 3:4:3 and Na$^+$ in isotropic (largely PSS) regions.*

$^{23}$Na NMR spectra of polymer films soaked in 1M NaCl solution were first acquired, and very different NMR signals were observed for the PEDOT:PSS film versus the PSS film alone (Figure 1d), the latter showing a single peak at -0.3 ppm with a full width at half maximum (FWHM) of 140 Hz. By contrast, the PEDOT:PSS film exhibits a triplet, comprising a central or isotropic (|+1/2> - |-1/2>) resonance and satellite (or outer (|+3/2> - |1/2>) and (|-3/2> - |-1/2>)) transitions. For $^{23}$Na, as a spin-3/2 quadrupolar nucleus, the position of the central transition remains unchanged while the outer transitions are affected, to first order, by the quadrupolar interaction with the local EFG, quantified via a quadrupolar coupling constant, $\chi$, leading to characteristic lineshapes that depend both on the $Na^+$ local environment and on any motion the $Na^+$ ions undergo.[30] When sodium ions hop rapidly between sites with random orientations, the quadrupolar interaction is averaged to zero, and a single $^{23}$Na NMR resonance is expected. This is the case for the PSS film, indicating that (i) the distribution of EFG tensor orientations which the sodium ions experience is isotropic and (ii) that the motion between the sites occupied by $Na^+$ in the film is rapid. When the sodium ions hop between environments with a non-random distribution of EFG tensors (an anisotropic medium), the quadrupolar interaction is no longer completely averaged. If all $Na^+$ ions sample the same anisotropic EFG distribution within the NMR timescale (ergodicity), this leads to a triplet of central and two satellite signals with a fixed intensity ratio of 3: 4: 3 and a frequency separation between the satellites, $\Delta\nu$, depending on the film orientation[30,31] as follows:

$$\Delta\nu = \frac{1}{2}\langle\bar{\chi}\rangle\,|3\,cos^2\,\theta - 1| \qquad (1)$$

where $\langle\bar{\chi}\rangle$ is the residual quadrupole coupling constant (RQCC) and $\theta$ is the angle between the magnetic field $B_0$ and the vector perpendicular (i.e., normal) to the film. $\Delta\nu$, as defined here, corresponds to twice the quadrupole splitting between the central line and each of the satellite peaks.

The triplet observed for this particular PEDOT:PSS film (Figure 1d) is typical for an anisotropic film structure with non-vanishing RQCC. However, the observed integral ratio in the triplet for this particular film is 0.22 : 0.56 : 0.22 (Figure 1d) and the relative intensity of the central peak increases as more NaCl solution is added to the polymer film (Figure S1). The additional intensity (comprising 29% of the total $^{23}$Na content for this film) is assigned to both $Na^+$ ions in the free electrolyte on top of the film and in the isotropic regions of the swollen film including PSS-rich and GOPS-containing region. This environment is referred to as "$Na^+$ in PSS" below, but strictly, it represents all the $Na^+$ ions located in isotropic media.

When the cast PEDOT:PSS film is rotated inside the NMR coil about the coil axis, the frequency separation, $\Delta\nu$, between the satellites changes as a function of the film orientation according to Eq. 1 yielding a value for $\langle\bar{\chi}\rangle$ of 4 kHz. The results indicate that the principal component of the (averaged) EFG tensor is also normal to the film providing strong evidence for a partial orientation of the polymer (pancake) nanostructure with respect to the substrate, as schematically illustrated in Figure 1c. The NMR spectrum taken of a wet PEDOT:PSS polymer film scraped of the glass substrate and randomly packed into an NMR tube gives a typical quadrupolar "powder" pattern, from which a similar $\langle\bar{\chi}\rangle$ value is extracted (Figure S1). The results clearly indicate that the $Na^+$ adsorption sites in the isotropic PSS-rich domains versus the anisotropic domains can be differentiated and quantified via $^{23}Na$ NMR spectroscopy. The anisotropic domains likely comprise both the PEDOT/PSS "pancakes" and nearby PSS polymer chains with partial ordering that originates from the film microstructure.

**Operando $^{23}Na$ NMR shows voltage-dependent changes in $Na^+$ concentration**

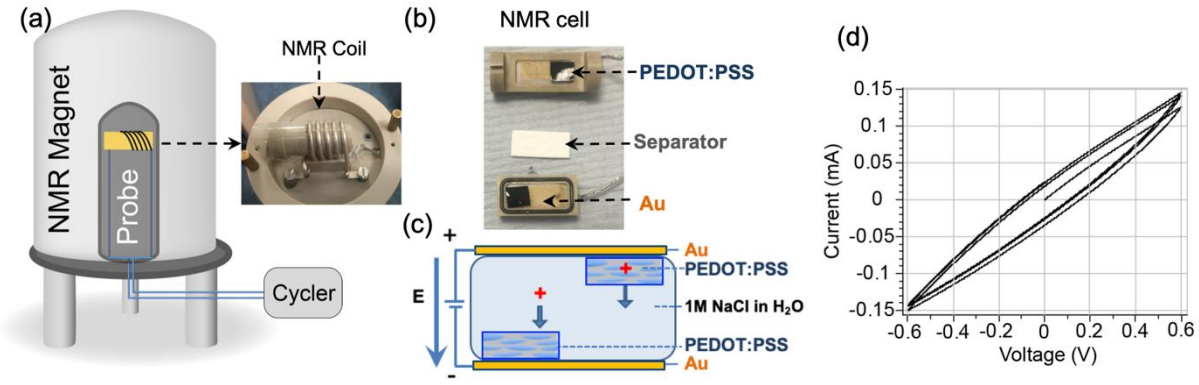


***Figure 2. Operando NMR setup**. (a) Schematic showing the operando NMR setup with a static probe connected to an electrochemical cycler. (b) Photo and (c) schematic of the symmetric NMR cell, which comprises two self-standing PEDOT:PSS films placed on Au meshes separated by a glass-fibre separator soaked with 1M NaCl aqueous electrolyte. (d) Cyclic voltammetry of the NMR cell scanned at 10 mV/s between -0.6V and 0.6V.*

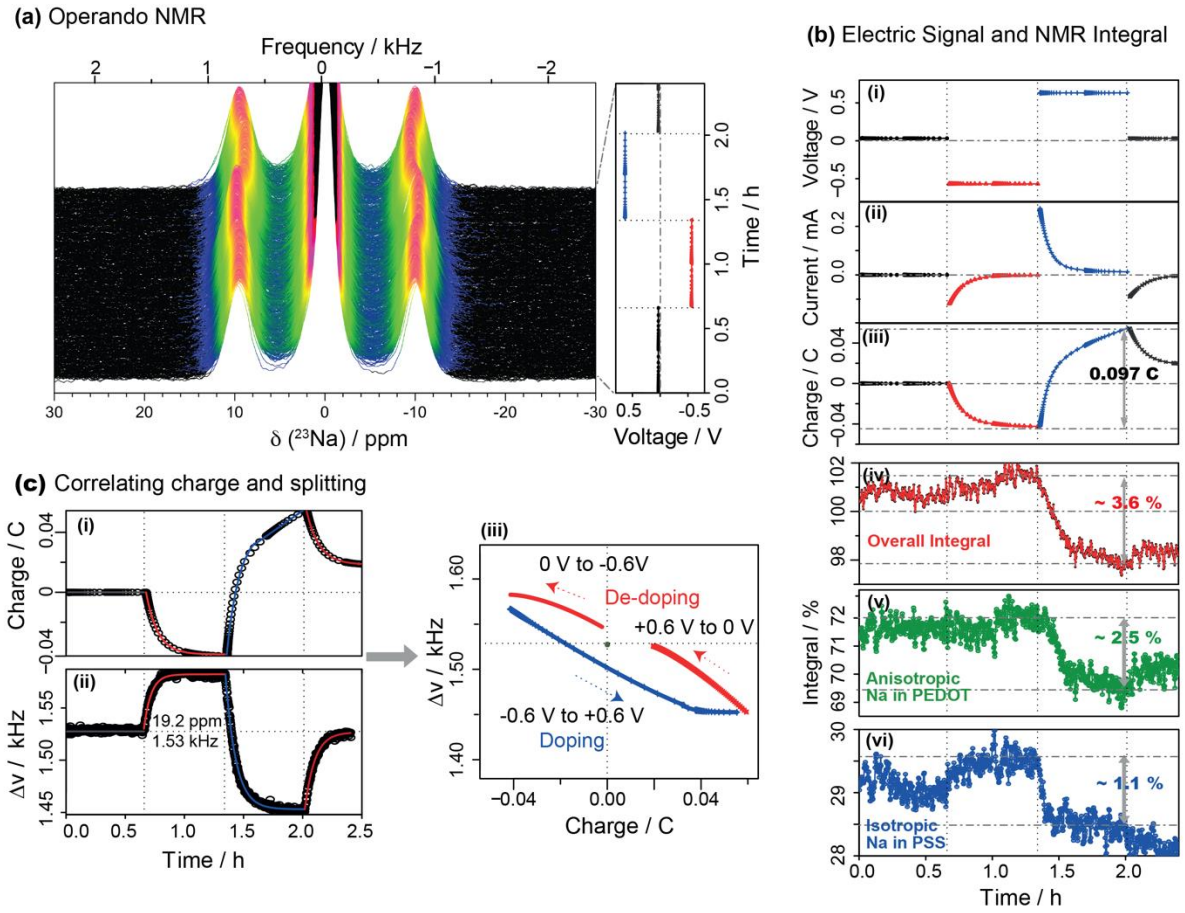


***Figure 3. Operando $^{23}$Na NMR spectra of 1.15 mm thick PEDOT:PSS film at potential holds from -0.6 to 0.6 V. (a)*** *$^{23}$Na NMR spectra acquired during the voltage holds (voltage profile shown on the right-hand side). Each spectrum takes about 10 s to acquire, while the voltage is held constant for 40 minutes at each step.* ***(b)*** *Electrochemistry and NMR peak integral analysis: (i) voltage-hold steps, (ii) current flow and (iii) charge (Q) removed/injected into the film vs. time, (iv) the corresponding total NMR integral, and integrals for (v) $Na^+$ in the PEDOT-rich (anisotropic) and (vi) PSS-rich (isotropic) region deconvoluted as illustrated in Figure 1g.* ***(c)*** *(i) Measured charge and (ii) $^{23}$Na NMR satellite separation ($\Delta\nu$) vs. time during the operando NMR study and (iii) correlation of charge and $\Delta\nu$.*

Operando NMR experiments were then performed to monitor the $Na^+$ ion movement in response to electrical doping/dedoping of the film, using a symmetric cell configuration similar to that developed to study supercapacitors[32] with two pieces of mass- and area-balanced PEDOT:PSS films (Figure 2b-c). Only one electrode is placed within the NMR coil, so that the ionic species injection/extraction can be individually monitored and quantified. The NMR cell was first activated by cyclic voltammetry to check the cell quality. At a scan rate of 10 mV/s, the electrochemical cell exhibited capacitive behaviour with no faradaic peaks (resulting from redox reactions) in the voltage window between -0.6 V and +0.6 V (Figure 2d).

Operando $^{23}Na$ NMR studies were performed by biasing the electrochemical cell to a constant voltage for 40 min, while 1D $^{23}Na$ NMR spectra were continuously recorded to monitor the $Na^+$ ion injection/extraction into/from the observed electrode (Figure 3). The current flowing through the cell decays during each of the voltage-hold steps, but even after 40 mins has not yet reached a steady state in the thick film used here, particularly on stepping the voltage from -0.6 to +0.6 V with respect to the electrolyte. Under negative bias, which leads to dedoping of the film, the $^{23}Na$ NMR quadrupolar splitting becomes larger (Figure 3c). The trend is opposite upon doping the film (i.e. on applying +0.6 V). A negative, close-to-linear correlation between the charge and satellite peak separation was found (Figure 3c-iii).

On applying a negative bias, $Na^+$ injection is expected if $Na^+$ is the major ionic charge compensating species. The total $^{23}Na$ NMR peak integral grows by approximately 1-2 % during PEDOT dedoping (0V→ -0.6V), but it drops more noticeably by 3.6% during doping (-0.6V→ +0.6V) as shown in Figure 3b-iii. The $^{23}Na$ NMR spectra were deconvoluted to separate the isotropic and anisotropic components as demonstrated in Figure 1e (shown in Figure 3b-iv and v, respectively), a voltage switch from -0.6V to +0.6V resulting in decrease of the signal from $Na^+$ ions in the PEDOT-rich (anisotropic) region by 2.5 %, the integral of $Na^+$ in PSS-rich region and electrolyte dropping more rapidly with time but by a smaller amount of 1.1 % (see Figure S5 for further analysis). The absolute intensity of the $^{23}Na$ NMR signal was calibrated to convert the NMR integral into the number of ions (Figure S6), the overall integral change corresponding to $8.1\times10^{-7}$ moles of $Na^+$, while the number of electrons removed from the polymer is 0.097 C (corresponding to $1.0\times10^{-6}$ moles of electrons, that is one hole in 28 to 41 EDOT units, and an estimated doping level of 2.4 – 3.5% per EDOT unit), leading to a $Na^+$-to-electron coupling efficiency of 81 % on doping.

When the voltage applied to the film increases stepwise from +/-0.2 V to +/-0.6 V, alternating between positive and negative voltages (Figure 4a), the resulting quadrupolar splitting also increases proportionally, increasing first at a voltage hold of - 0.2 V and then decreasing when the voltage is stepped to +0.2 V. A negative linear correlation between charge and splitting was again observed as shown in Figure S14b in SI. The voltage hold time used however are much shorter, and the system no longer has time to equilibrate. This is particularly pronounced on switching from negative to positive voltages, since in contrast to the positive to negative step, no 0 V hold step was applied. Consequently, more charge is injected into the film than removed, which is accompanied by a steady increase in the $^{23}Na$ intensity. Similar trends are observed in Figure 4b where a lower biasing voltage of +/-0.4 V is used. $^{23}Na$ NMR integral

changes observed for the films in Figure 4a and b were analysed, and the corresponding $Na^+$-to-electron coupling efficiency varies between 63 and 135 % depending on the exact cycling history of the film (Figure S7).

A thinner (0.35 mm thick) PEDOT:PSS film was prepared in the same way to more closely mimic films in real devices and its operando NMR data is shown in Figure 4c. Both the charge and $^{23}Na$ quadrupolar splitting change much more rapidly in response to the alternating voltage than seen for the 1.15 mm thick film, and the same negative trend in quadrupolar splitting vs. charge is seen (Figure S9g).

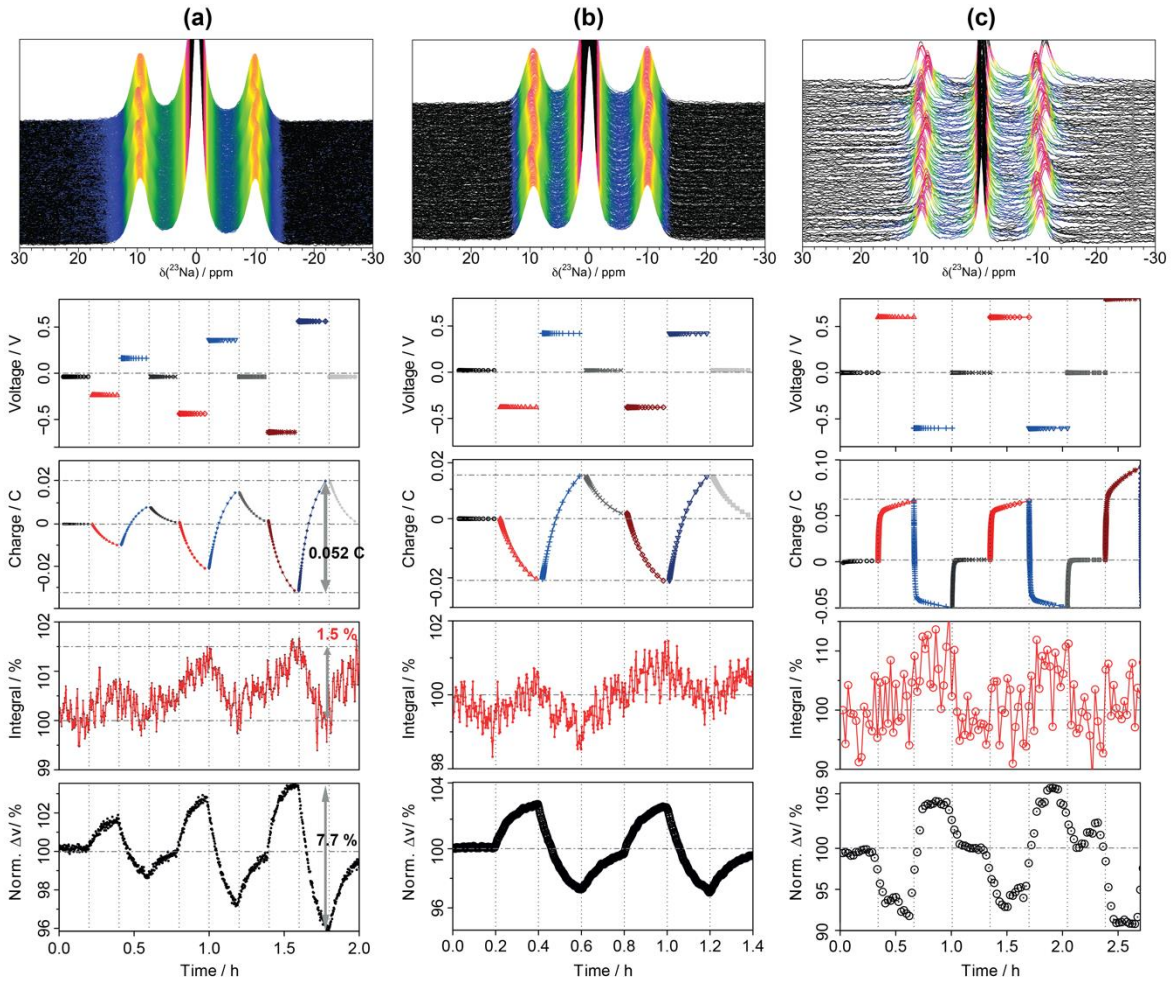


***Figure 4. Operando $^{23}Na$ NMR of thick (1.15 mm) PEDOT:PSS film (a-b) and thin (0.35 mm) PEDOT:PSS film (c) biased to different voltages.*** *The measured satellites separation, $\Delta\nu$, was normalized by $(\Delta\nu - \Delta\nu_0)/\Delta\nu_0$ where $\Delta\nu_0$ corresponds to the initial value without voltage biasing.*

**Operando $^1$H NMR reveals water movement**

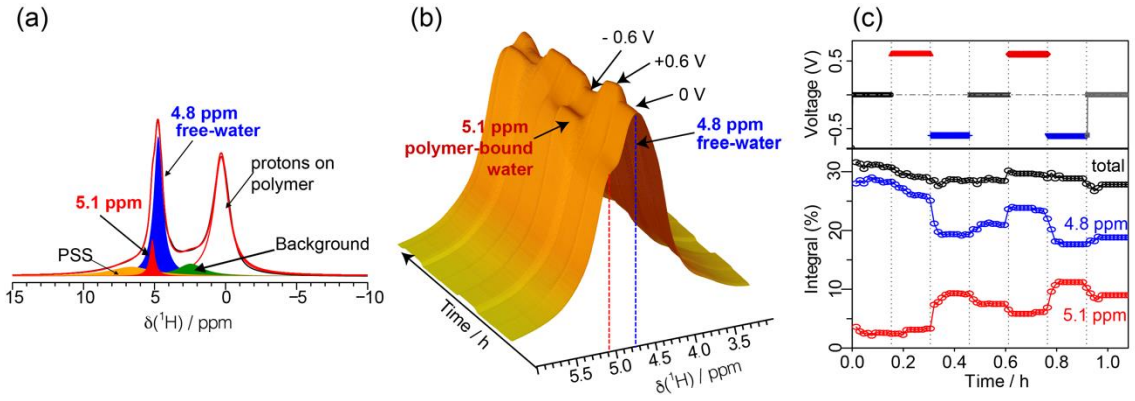


***Figure 5 Operando $^1$H NMR of the 0.35 mm PEDOT:PSS film.*** *(a) $^1$H NMR spectrum with peak deconvolution. (b) 3D plot of the operando $^1$H NMR data with key resonances and voltages marked. (c) Voltage-hold history and the peak integral trend of the deconvoluted peaks centred at 4.8 ppm (blue), 5.1 ppm (red) and their total integral (black). In (a) the broad component centred around 2 ppm (coloured in green) is assigned to the background proton signal from the operando cell (made of PEEK). The other broad signal centred around 7 ppm (coloured in yellow) rises from the protons on the styrene sulfonate group in the PSS polymer (where the broadening is mainly due to the strong $^1$H dipolar coupling).*

Operando $^1$H NMR experiments were performed to monitor the movement of water into the hydrated polymer during voltage-biasing (Figure 5). The $^1$H NMR spectrum of the PEDOT:PSS thin film (Figure 5a) has two intense, broad peaks at around 0.2 ppm (assigned to aliphatic protons originating from the PSS chains and GOPS cross-linker) and at 4.8 ppm, the latter having a shoulder at 5.1 ppm. The $^1$H signal at 4.8 ppm (shaded in blue) is assigned to free water in the electrolyte and the 5.1 ppm shoulder peak (shaded in red) is assigned to water in polymer regions based on its chemical shift.[33] The height (and integral) of the 4.8 ppm peak increases at positive voltage-biasing and decreases at negative voltage. A switch from +0.6 V to -0.6 V leads to a sharp increase of the 5.1 ppm peak integral, while the total water integral (4.8 + 5.1 ppm) does not change noticeably (Figure 5c), the results suggesting that during dedoping water diffuses into the polymer, likely in the form of hydrated cations. This result agrees well with a previous study by Savva et al.,[22] who showed that PEDOT:PSS films undergo significant volumetric expansion during dedoping due to uptake not only of cations but also of water.[34] The volume expansion pushes water out of the area sampled by the NMR coil, reducing the intensity of the 4.8 ppm signal. Note that each $^1$H NMR spectrum takes about 48 s to acquire and the rapid change of $^1$H NMR spectra as a function of voltage indicates that the hydration speed of the film is within one or two minutes, which is faster than many other common hydrogels.[35]

An initial (inconclusive) attempt to monitor the anion movement by operando $^{35}$Cl NMR is shown in Figure S16 in the SI. The signal-to-noise of the $^{35}$Cl NMR spectra was poor due to the low sensitivity of $^{35}$Cl nucleus, and the operando data do not show noticeable changes.

**Discussion:**

**Physical Interpretation of $^{23}$Na NMR quadrupolar splitting – charge correlation**

The asymmetric charge distribution around the $Na^+$ ions is measured here via $^{23}$Na NMR spectroscopy, and satellite separations $\Delta\nu$ of the order of 2–4 kHz are observed for the wet PEDOT:PSS film, corresponding to a RQCC ($\langle\bar{\chi}\rangle$) of 4 kHz (see Eq.1). This is much smaller than the quadrupolar coupling constant of 1.3 MHz measured via Multiple Quantum Magic Angle Spinning (MQMAS) NMR for the $Na^+$ ions bound to sulfonate groups in dry Na-PSS powder (Figure S3). This difference is ascribed to the fast exchange or hopping between free and bound states (e.g., $SO_3^-$ moieties) with weak (or zero) and strong EFGs, respectively, and between bound states with different orientations of their EFG tensors with respect to the static magnetic field. Furthermore, a non-zero $\langle\bar{\chi}\rangle$ indicates that there is an underlying preferred orientation of the environments of the bound states, consistent with the pancake structures of the PEDOT-rich regions. Similar small residual quadrupole coupling constants have previously been reported for liquid crystals[36], co-polymers[37], and hydrated biological samples[38], in cases where local orderings are present. The zero value of $\langle\bar{\chi}\rangle$ observed for $Na^+$ in the PSS-regions, or indeed in the PSS-only films, indicates that the $SO_3^-$ moieties (in these regions) are oriented randomly with respect to the magnetic field. The change in the quadrupole splitting seen here on biasing the films is not simply a direct consequence of the applied voltage and the resulting electric field between, for example, the electrodes in the cell. Rather than responding instantaneously to the stepped voltage changes, the NMR-observed splitting closely follows the holes injected or removed from the system as measured with voltage holds at different fixed potentials (Figures 3 and 4).

A key feature of PEDOT:PSS is that the amount of $SO_3^-$ available for $Na^+$ binding is controlled by the number of holes on PEDOT, i.e. the level of doping of the film. By assuming that the binding of holes to $SO_3^-$ (as illustrated in Figure 1a) is strong (and dictated by local charge balancing/neutrality) whereas the $Na^+$ binding to $SO_3^-$ is weaker, an expression for the satellite separation $\Delta\nu$ and thus $\langle\bar{\chi}\rangle$ as a function of the charge (Q) delivered to PEDOT:PSS can be readily derived (see SI section 6 for derivation and assumptions):

$$\langle \bar{\chi} \rangle = K_{Na} \left( [SO_3^-]_O - [h^+]_O^0 - \frac{Q}{F\, f\, V_{film}} \right) S\, \chi \qquad (2)$$

with $K_{Na}$ the binding equilibrium constant between $Na^+$ and $SO_3^-$ groups at the PEDOT/PSS interfaces defined in Eq. S2a in SI. $[SO_3^-]_O$ and $[h^+]_O$ are the total sulfonate and hole concentrations, respectively, in the PEDOT:PSS regions, $V_{film}$ the volume of the polymer film, $f$ the volumetric fraction of the PEDOT-PSS pancakes in the film and F the Faraday constant. S is an order parameter reflecting the average orientation of the PSS polymer chains in the PEDOT-PSS regions of the film (illustrated in Figure S12 and defined in Eq. S8 in the SI), $\chi$ is the $^{23}Na$ quadrupole coupling constant of the ion in the bound state, in the absence of any motion. Assuming other parameters are constant, Eq. 1 and 2 together predicts a linear relation between charge, Q and splitting, which is indeed what is approximately observed (Figure 3c-iii, Figure 4 and Figure S14).

A model with weak binding of $Na^+$ to the $SO_3^-$ groups that are not bound to the holes is supported by a number of observations including: first, the quadrupolar splitting increases when the concentration of the NaCl solution increases (Figure S4), the higher concentration of $Na^+$ ions shifting the binding equilibrium towards increased $Na^+$-$SO_3^-$ binding and secondly, $\langle \bar{\chi} \rangle$ tracks the charge almost instantaneously, doping of PEDOT almost instantaneously reducing the number of $SO_3^-$ binding sites available for $Na^+$. It should be kept in mind that while this binding model considers holes to be tightly bound to $SO_3^-$ groups, the holes themselves can still be mobile. This is not inconsistent with the energy level structure of PEDOT:PSS. Holes in degenerately doped organic semiconductors occupy a transport manifold that originates from highest occupied molecular orbitals of the conjugated system and is broadened due to positional and electrostatic disorder – the latter arising in part by the strong dipolar interactions between holes and dopants ($SO_3^-$ in this case).[39,40] As a result, holes close to the Fermi level will be highly mobile, while those at the tail of the manifold near the band gap will be essentially trapped. However, as the film is dedoped and the Fermi level approaches the edge of the transport manifold, these holes will also become mobile albeit with a lower mobility.[41] The results presented here show that the $Na^+$ ions themselves are also mobile and in rapid equilibrium with the $SO_3^-$ groups and thus can readily respond to maintain local charge neutrality as the holes move.

**Ion dynamics**

The curves of $\langle \bar{\chi} \rangle$ vs. the hold time at different voltages can be fit with an exponential decay function using the equation: $\mathrm{A} \times exp\left(-\frac{t}{\tau}\right) + B$, yielding values of $\tau$ that vary from 20-400 s

depending on film thickness (Figure S9 and S10). The average $\tau$-value is 355 s for the thick film and 22 s for the thin film. A self-diffusion coefficient of the $Na^+$ ion in the films was measured by $^{23}Na$ pulsed field gradient (PFG) NMR to be $1.13\times10^{-5}$ $cm^2\ s^{-1}$ (Figure S11), which corresponds to a drift mobility of $4.40\times10^{-4}$ $cm^2\ s^{-1}V^{-1}$ that it is in the same order of magnitude of the drift mobility reported by Stavrinidou et al.[19] Assuming a 1D ion diffusion process, the root of the mean-squared displacement of the $Na^+$ ions during the time periods of $\tau$ is 0.90 mm for thick film and 0.23 mm for thin film, the values of which are comparable to the film thicknesses (1.15 mm and 0.35 mm, respectively). This analysis suggests that the charge injection and the resultant change in $\langle\bar{\chi}\rangle$ do reflect the ion redistribution process within the film.

The NMR intensity changes seen on doping (Figure 3b iv-vi and Figure S5) provide insight concerning the ion dynamics within the film. When holes are injected, this is immediately detected by $^{23}Na$ NMR spectroscopy as fewer ions now bind on average to the PSS/PEDOT interfaces and the quadrupolar splitting decreases. However, the intensity of the anisotropic component of signal does not respond as quickly, as it takes a finite time for the displaced ions to drift out of the pancake (anisotropic) region. Charge neutrality must, however, be achieved and the more highly mobile (but more distant) $Na^+$ ions and possibly protons are the first to leave the film, as manifested by the faster NMR intensity decay for the $Na^+$ signal from the PSS region. The general migration of the (hydrated) ions in and out of the film is also seen via the changes in $^1H$ signal intensity.

**Origin of the hysteresis**

The discussion above develops a model that predicts a linear correlation between charge and splitting; however, the experimental data shows a degree of hysteresis and some deviation from the simple linear correlation (Figure 3c and Figure S14), likely due to other parameters that are not considered within this model. The first set of phenomena to consider, are the parasitic reactions that are seen during voltage-holding periods, particularly at higher voltages. A clear indicator of this is the almost constant value of $\Delta v$ seen after approximately 0.04 C of charge has been injected on stepping the voltage to +0.6 V (Figure 3c), current still being measured beyond this point. This is the explored in the SI (Figure S6-ii), the analysis showing that the current flow vs. time plots could not be fit with the simple exponential used above ($\mathrm{A}\times exp\left(-\frac{t}{\tau}\right)+B$) when a hold voltage of 0.6 V is used but could be modelled by including a Faradaic process that is presumed to be linear in time (as shown in Figure S9, S10). The contribution to the charge from Faradaic (parasitic) processes drops when the films are only charged to +/- 0.2 and 0.4 V, suggesting that the parasitic reactions can be mitigated by using

appropriate voltage windows. One possible source of these parasitic reactions is the reduction of dissolved oxygen by dedoped $PEDOT^0$ to form $H_2O_2$.[21,42]

Other factors include possible changes in the PSS binding site local environment that might occur during doping/dedoping, resulting in changes in $\chi$. Since the measured residual value of $\chi$, $\langle\bar{\chi}\rangle$, is also affected by the shape of the PEDOT-rich domains (as illustrated in Figure S12), the hysteresis may be caused by microstructural changes of the PEDOT:PSS (quantified via the order parameter, S) during electrochemical biasing, such as film swelling due to changes in water content. Other phenomena might be important: for example, Paulsen et al.[43] recently reported an unsymmetric rate of structural change of PEDOT:PSS during doping and dedoping by operando X-ray scattering, ascribing the transient structural behaviour to the complex polaron-bipolaron dynamics that affects electronic charge carrier dynamics.

Finally, $^{23}Na$ NMR integral changes with biasing show a dependence on cycling history. When parasitic (Faradaic) process is deducted from the observed charge, some experiments show $Na^+$-to-electron coupling efficiencies of close to 98 % (Figure S6). However, this strong coupling efficiency is not always seen, some experiments showing a greater increase in Na NMR integral than expected based on this charge passed (Figure S7a). We ascribe these observations to competitive binding of $Na^+$ vs. $H^+$ to the sulfonate groups in PSS, the $H^+$ ions hoping more rapidly and likely responding more quickly to changes in voltage bias. The anions may also play a role, which cannot be excluded until better signal-to-noise ratio $^{35}Cl$ NMR spectra can be acquired.

**Conclusions:**

$^{23}Na$ and $^{1}H$ NMR spectroscopy were used to study ionic gating of PEDOT:PSS aqueous films. Via $^{23}Na$ NMR, we differentiate between two sodium environments. The first involves $Na^+$ in the PSS-rich matrix, which gives rise to a single peak indicating that (i) the $Na^+$ ions are highly mobile and (ii) the $SO_3^-$ moieties on the PPS chains are randomly oriented in the film. The second environment is assigned to $Na^+$ ions in and nearby the PEDOT-rich regions and gives rise to a triplet in the $^{23}Na$ NMR spectrum. This triplet indicates that the ions experience a residual EFG (and thus non-zero residual quadrupolar coupling constant, $\langle\bar{\chi}\rangle$) that depends on the orientation of the film to the static magnetic field, confirming that the film comprises highly ordered microstructures – or “pancakes” - oriented parallel to the film substrate.

A negative linear correlation between $\langle\bar{\chi}\rangle$, and the charge stored within the film, was observed in the operando $^{23}Na$ NMR measurements. This was interpreted via a competitive binding

model, where the size of $\langle\bar{\chi}\rangle$ was determined by the number of bound $Na^+$ ions near the PEDOT/PSS interface and the degree of chain ordering. The number of binding sites varies linearly with hole concentration on PEDOT, thus modulating $\langle\bar{\chi}\rangle$. Operando $^1H$ NMR spectroscopy clearly revealed that water molecules accompany the cation insertion and removal from the films on gating the voltage.

The value measured for the diffusion coefficient of the $Na^+$ ions in the films is consistent with the timescales that accompany charge injection and ion migrations in these films, the process involving rapid removal of $Na^+$ ions in the PSS-rich matrix and slower removal of ions from the PEDOT-rich regions. Quantification of the $Na^+$-to-electron coupling efficiency yields values that are consistently above 63% for PEDOT:PSS, the exact values depend on the prior voltage cycling history of the film. This relatively high coupling efficiency confirms that while $Na^+$ is not the only ionic charge carrier, it is the major ionic species compensating the charge, at least under the current experimental conditions. Future work will focus on improving the sensitivity of the $^{35}Cl$ NMR spectroscopy, and on acquiring operando $^1H$ and $^{23}Na$ NMR spectra simultaneously on the same sample to quantify the relative molar ratios of injected $Na^+$ and $H_2O$.

The operando NMR method opens new route to obtain quantitative insights on alkaline ion dynamics in organic mixed conductors. The method developed here can be extended to study next-generation organic mixed conductors and their interactions with electrolytes. Multinuclear operando NMR of alkaline cations such as ($^7Li$, $^{23}Na$, $^{87}Rb$, $^{133}Cs$) or anions bearing NMR-active nuclei ($^{19}F$,$^{35/37}Cl$, $^{79/81}Br$, $^{127}I$) as well as deuterated water could be further utilized to understand the ionic motion and their interaction with the polymer, so that a structure-property relationship can be established during device operation.

**Experiments:**

**Materials**

PEDOT:PSS (Clevios PH1000, Heraeus Holding GmbH) was mixed with 1 wt % 3-glycidoxypropyltrimethoxysilane (GOPS, Sigma-Aldrich). Then the mixture was sonicated for 10 minutes and was filtered through a 0.45 µm polyvinylidene fluoride (PVDF) filter into a plastic petri dish with diameter of 9.5 cm. The mixture was then heated at 70˚C for 12 h. For thin and thick films, 10 ml and 20 ml of PEDOT:PSS solution was used, respectively. After heating the film was fully dried and was soaked in deionized (DI) water for 8 h for rehydration, then it was rinsed with DI water for three times (each with 1 h soaking) to remove uncross-linked components. The hydrated film was soaked in 1M NaCl solution for 12 h, then rinsed

with 1M NaCl solution (with 1 h soaking) for three times in order to reach a concentration equilibrium between the solution and the film before NMR measurement. The PSS film was prepared in the same way by cross-linking PSSNa (Sigma-Aldrich, Mw ~70,000) with GOPS, and was rinsed with DI water and soaked in 1M NaCl solution.

**NMR cell assembly**

The photo of the symmetric cell used for NMR measurement are shown in Figure 2b. It consists of gold mesh (0.5 cm x 1.2 cm, from Sigma GF14297430, thickness 0.004 mm), and two self-standing PEDOT:PSS films (approximately 0.5 cm x 0.5 cm in dimension with thickness of 0.35 mm or 1.15 mm) separated by borosilicate glass fibre (Whatman, GF/A). The electrolyte was 1 M NaCl in DI water. One of the electrodes is placed inside the NMR coil to be monitored. The details about the cell designed can be found in Ref.[27] Cyclic voltammetry (CV) was performed using a Biologic SP-100 potentiostat to check the quality of the symmetric cell before and after operando NMR experiments.

**Operando solid-state NMR**

NMR experiments were performed using a Bruker Avance spectrometer operating at a magnetic field strength of 7.05 T, corresponding to $^{1}$H and $^{23}$Na Larmor frequencies of 300 and 79.4 MHz, respectively. In-house designed static probes with automatic tuning (ATMC) and matching capabilities and a double resonance (DR) probe (along with connections for an external battery cycler) were used for the measurements. The NMR coil used in this study was a 5-turn silver coated Cu solenoidal coil with a diameter of 11 mm. The electrochemical cell was aligned such that the electrodes were parallel to the applied field for operando measurement. In order to maximise the signal-to-noise ratio for the time-restricted measurement, single-pulse experiments were used for both $^{1}$H and $^{23}$Na NMR experiments. Operando $^{23}$Na NMR data of the thin PEDOT:PSS film (0.35 mm) were acquired on a DR probe using a 90° pulse corresponded to 10 μs (mutation frequency of 25 kHz) at 100 W with 256 transients and a recycle delay of 0.25 s (around 1 min per spectrum). The signal-to-noise ratio of the thick PEDOT:PSS film (1.15 mm) was much better than thin film, thus, only 32 transients were used (around 10 s per spectrum). The spin-lattice ($T_1$) relaxation of the $^{23}$Na NMR signals were measured to be 33 ms using saturation recovery pulse sequence. The recycle delay of 0.2 s used here is sufficient-long for quantitative information.

Operando $^{1}$H NMR data of the thin PEDOT:PSS film (0.35 mm) were acquired on DR probe using a 90° pulse corresponded to 12 μs at 100 W with 16 transients and a recycle delay of 3 s (around 48 s per spectrum). $^{23}$Na NMR and $^{1}$H NMR spectra were referenced to 1 M NaCl

in $H_2O$ at 0 ppm and 4.8 ppm, respectively. Electrochemical measurements were performed using a Biologic VSP potentiostat by applying a constant voltage (versus the open circuit voltage) to cells. The NMR spectra were processed in Bruker Topspin software and further peak deconvolution and data processing was performed with R scripts.

**Acknowledgements**

Y.J thanks the useful discussion with Prof. Yong Yang, Dr. Pedro Braga Groszewicz, Dr. David M. Halat and Yuning Zhou. Y. J acknowledges Dr. Chris M. Proctor and Anastasios Polyravas for advising on the PEDOT:PSS film preparation. Y.J and C.P.G. acknowledge funding support from EPSRC under grant number EP/M009521/1. We thank Dr Oliver Pecher for assistance with the NMR hardware. S.S. acknowledges support from the CCP for NMR Crystallography and EPSRC grant EP/M022501/1.

**References:**

(1) Someya, T.; Bao, Z.; Malliaras, G. G. *Nature* **2016**, *540* (7633), 379–385.

(2) Paulsen, B. D.; Tybrandt, K.; Stavrinidou, E.; Rivnay, J. *Nat. Mater.* **2020**, *19*, 13–26.

(3) Peng, C.; Ning, G. H.; Su, J.; Zhong, G.; Tang, W.; Tian, B.; Su, C.; Yu, Di.; Zu, L.; Yang, J.; Ng, M. F.; Hu, Y. S.; Yang, Y.; Armand, M.; Loh, K. P. *Nat. Energy* **2017**, *2*, 17074.

(4) Wu, F.; Liu, J.; Li, L.; Zhang, X.; Luo, R.; Ye, Y.; Chen, R. *ACS Appl. Mater. Interfaces* **2016**, *8* (35), 23095–23104.

(5) Wu, M.; Xiao, X.; Vukmirovic, N.; Xun, S.; Das, P. K.; Song, X.; Olalde-Velasco, P.; Wang, D.; Weber, A. Z.; Wang, L. W.; Battaglia, V. S.; Yang, W.; Liu, G. *J. Am. Chem. Soc.* **2013**, *135*, 12048–12056.

(6) Rivnay, J.; Inal, S.; Salleo, A.; Owens, R. M.; Berggren, M.; Malliaras, G. G. *Nature Reviews Materials*. **2018**, *3*, p 17086.

(7) Andersson Ersman, P.; Lassnig, R.; Strandberg, J.; Tu, D.; Keshmiri, V.; Forchheimer, R.; Fabiano, S.; Gustafsson, G.; Berggren, M. *Nat. Commun.* **2019**, *10* (1), 1–9.

(8) Gkoupidenis, P.; Schaefer, N.; Garlan, B.; Malliaras, G. G. *Adv. Mater.* **2015**, *27* (44), 7176–7180.

(9) Van De Burgt, Y.; Lubberman, E.; Fuller, E. J.; Keene, S. T.; Faria, G. C.; Agarwal, S.; Marinella, M. J.; Alec Talin, A.; Salleo, A. *Nat. Mater.* **2017**, *16* (4), 414–418.

(10) Berggren, M.; Malliaras, G. G. *Science* **2019**, *364* (6437), 233–234.

(11) Elschner, A., Kirchmeyer, S., Merker, U., Lovenich, W., & Reuter, K. *PEDOT: Principles and Applications of an Intrinsically Conductive Polymer*; CRC Press, 2010.

(12) Nardes, A. M.; Kemerink, M.; Janssen, R. A. J.; Bastiaansen, J. A. M.; Kiggen, N. M. M.; Langeveld, B. M. W.; Van Breemen, A. J. J. M.; De Kok, M. M. *Adv. Mater.* **2007**, *19* (9), 1196–1200.

(13) Rivnay, J.; Inal, S.; Collins, B. A.; Sessolo, M.; Stavrinidou, E.; Strakosas, X.; Tassone, C.; Delongchamp, D. M.; Malliaras, G. G. *Nat. Commun.* **2016**, *7* (1), 1–9.

(14) Timpanaro, S.; Kemerink, M.; Touwslager, F. J.; De Kok, M. M.; Schrader, S. *Chem. Phys. Lett.* **2004**, *394* (4–6), 339–343.

(15) Lenz, A.; Kariis, H.; Pohl, A.; Persson, P.; Ojamäe, L. *Chem. Phys.* **2011**, *384* (1–3), 44–51.

(16) Takano, T.; Masunaga, H.; Fujiwara, A.; Okuzaki, H.; Sasaki, T. *Macromolecules* **2012**, *45* (9), 3859–3865.

(17) Kim, Y. H.; Sachse, C.; MacHala, M. L.; May, C.; Müller-Meskamp, L.; Leo, K. *Adv. Funct. Mater.* **2011**, *21* (6), 1076–1081.

(18) Inal, S.; Rivnay, J.; Suiu, A. O.; Malliaras, G. G.; McCulloch, I. *Acc. Chem. Res.* **2018**, *51* (6), 1368–1376.

(19) Stavrinidou, E.; Leleux, P.; Rajaona, H.; Khodagholy, D.; Rivnay, J.; Lindau, M.; Sanaur, S.; Malliaras, G. G. *Adv. Mater.* **2013**, *25* (32), 4488–4493.

(20) Mantione, D.; del Agua, I.; Sanchez-Sanchez, A.; Mecerreyes, D. *Polymers (Basel).* **2017**, *9* (8), 354.

(21) Mitraka, E.; Gryszel, M.; Vagin, M.; Jafari, M. J.; Singh, A.; Warczak, M.; Mitrakas, M.; Berggren, M.; Ederth, T.; Zozoulenko, I.; Crispin, X.; Głowacki, E. D. *Adv. Sustain. Syst.* **2019**, *3* (2), 1800110.

(22) Savva, A.; Wustoni, S.; Inal, S. *J. Mater. Chem. C* **2018**, *6* (44), 12023–12030.

(23) Forse, A. C.; Griffin, J. M.; Merlet, C.; Carretero-Gonzalez, J.; Raji, A.-R. O.; Trease, N. M.; Grey, C. P. *Nat. Energy* **2017**, *2*, 16216.

(24) Jin, Y.; Kneusels, N.-J. H.; Magusin, P. C. M. M.; Kim, G.; Castillo-Martinez, E.;

Marbella, L. E.; Kerber, R. N.; Howe, D. J.; Paul, S.; Liu, T.; Grey, C. P. *J. Am. Chem. Soc.* **2017**, *139* (42), 14992–15004.

(25) Jin, Y.; Kneusels, N.-J. H.; Marbella, L. E.; Castillo-Martinez, E.; Magusin, P. C. M. M.; Weatherup, R. S.; Jonsson, E.; Liu, T.; Paul, S.; Grey, C. P. *J. Am. Chem. Soc.* **2018**, *140*, 9854−9867.

(26) Jin, Y.; Kneusels, N. J. H.; Grey, C. P. *J. Phys. Chem. Lett.* **2019**, *10* (20), 6345–6350.

(27) Pecher, O.; Carretero-Gonzalez, J.; Griffith, K. J.; Grey, C. P. *Chemistry of Materials*. 2017, 29, pp 213–242.

(28) Slichter, C. P. In *Principles of Magnetic Resonance*; Springer Berlin Heidelberg: Berlin, Heidelberg, 1990; pp 485–502.

(29) Sturniolo, S.; Green, T. F. G.; Hanson, R. M.; Zilka, M.; Refson, K.; Hodgkinson, P.; Brown, S. P.; Yates, J. R. *Solid State Nucl. Magn. Reson.* **2016**, *78*, 64–70.

(30) Man, P. P.; Klinowski, J.; Trokiner, A.; Zanni, H.; Papon, P. *Chem. Phys. Lett.* **1988**, *151* (1–2), 143–150.

(31) Philp, D. J.; Naumann, C.; Kuchel, P. W. *Concepts Magn. Reson. Part A* **2012**, *40A* (2), 90–99.

(32) Wang, H.; Forse, A. C.; Griffin, J. M.; Trease, N. M.; Trognko, L.; Taberna, P. L.; Simon, P.; Grey, C. P. *J. Am. Chem. Soc.* **2013**, *135* (50), 18968–18980.

(33) Gun'ko, V.; Savina, I.; Mikhalovsky, S. *Gels* **2017**, *3* (4), 37.

(34) Savva, A.; Cendra, C.; Giugni, A.; Torre, B.; Surgailis, J.; Ohayon, D.; Giovannitti, A.; McCulloch, I.; Di Fabrizio, E.; Salleo, A.; Rivnay, J.; Inal, S. *Chem. Mater.* **2019**, *31* (3), 927–937.

(35) Lu, B.; Yuk, H.; Lin, S.; Jian, N.; Qu, K.; Xu, J.; Zhao, X. *Nat. Commun.* **2019**, *10*, 1043.

(36) Lindblom, G. *Acta Chem. Scand. A.* **1972**, *26*, 1745–1748.

(37) Grundy, L. S.; Sethi, G. K.; Galluzzo, M. D.; Loo, W. S.; Maslyn, J. A.; Teran, A. A.; Thelen, J. L.; Timachova, K.; Reimer, J. A.; Madsen, L. A.; Balsara, N. P. *ACS Macro Lett.* **2019**, *8* (2), 107–112.

(38) Eliav, U.; Navon, G. *NMR Biomed.* **2016**, *29* (2), 144–152.

(39) Shen, Y.; Diest, K.; Wong, M. H.; Hsieh, B. R.; Dunlap, D. H.; Malliaras, G. *Phys. Rev. B - Condens. Matter Mater. Phys.* **2003**, *68* (8), 1–4.

(40) Arkhipov, V. I.; Emelianova, E. V; Heremans, P.; Bässler, H. *Phys. Rev. B* **2005**, *72* (23), 235202.

(41) Tanase, C.; Blom, P. W. M.; De Leeuw, D. M.; Meijer, E. J. *Phys. Status Solidi Appl. Res.* **2004**, *201* (6), 1236–1245.

(42) Gueskine, V.; Singh, A.; Vagin, M.; Crispin, X.; Zozoulenko, I. *J. Phys. Chem. C* **2020**, *124* (24), 13263–13272.

(43) Paulsen, B. D.; Wu, R.; Takacs, C. J.; Steinrück, H.-G.; Strzalka, J.; Zhang, Q.; Toney, M. F.; Rivnay, J. *Adv. Mater.* **2020**, *32* (40), 2003404.

## Supplementary Files

This is a list of supplementary files associated with this preprint. Click to download.

- PEDOTPSSSupportingInformation.docx